JACC: CARDIOVASCULAR IMAGING
VOL. 4, NO. 12, 2011

ISSN 1936-878X/$36.00
PUBLISHED BY ELSEVIER INC.
DOI:10.1016/j.jcmg.2011.08.016

CVN Interview

Detection and Quantification of Myocardial Reperfusion Hemorrhage Using T2*-Weighted CMR

Andreas Kumar, MD, MSc,* Jordin D. Green, PhD,†‡ Jane M. Sykes, RVT,§ Pinhas Ephrat, MSc,§ Jeffrey J. L. Carson, PhD,§ Andrea J. Mitchell, BSc,§ Gerald Wisenberg, MD,§ Matthias G. Friedrich, MD†

Québec City, Québec, Calgary, Alberta, and London, Ontario, Canada

OBJECTIVES The purpose of this study was to validate T2*-weighted cardiac magnetic resonance (T2*-CMR) for the detection and quantification of reperfusion hemorrhage in vivo against an ex vivo gold standard, and to investigate the relationship of hemorrhage to microvascular obstruction, infarct size, and left ventricular (LV) functional parameters.

BACKGROUND Hemorrhage can contribute to reperfusion injury in myocardial infarction and may have significant implications for patient management. There is currently no validated imaging method to assess reperfusion hemorrhage in vivo. T2*-CMR appears suitable because it can create image contrast on the basis of magnetic field effects of hemoglobin degradation products.

METHODS In 14 mongrel dogs, myocardial infarction was experimentally induced. On day 3 post-reperfusion, an in vivo CMR study was performed including a T2*-weighted gradient-echo imaging sequence for hemorrhage, standard sequences for LV function, and post-contrast sequences for microvascular obstruction and myocardial necrosis. Ex vivo, thioflavin S imaging and triphenyltetrazoliumchloride (TTC) staining were performed to assess microvascular obstruction, hemorrhage, and myocardial necrosis. Images were analyzed by blinded observers, and comparative statistics were performed.

RESULTS Hemorrhage occurred only in the dogs with the largest infarctions and the greatest extent of microvascular obstruction, and it was associated with more compromised LV functional parameters. Of 40 hemorrhagic segments on TTC staining, 37 (92.5%) were positive for hemorrhage on T2*-CMR (kappa $= 0.96$, $p < 0.01$ for in vivo/ex vivo segmental agreement). The amount of hemorrhage in 13 affected tissue slices as determined by T2*-CMR in vivo correlated strongly with ex vivo results ($20.3 \pm 2.3\%$ vs. $17.9 \pm 1.6\%$ per slice; Pearson $r = 0.91$; $r^2 = 0.83$, $p < 0.01$ for both). Hemorrhage size was not different between in vivo T2*-CMR and ex vivo TTC (mean difference $2.39 \pm 1.43\%$; $p = 0.19$).

CONCLUSIONS T2*-CMR accurately quantified myocardial reperfusion hemorrhage in vivo. Hemorrhage was associated with more severe infarct-related injury. (J Am Coll Cardiol Img 2011;4: 1274–83) © 2011 by the American College of Cardiology Foundation

From the *Québec Heart and Lung Institute, Laval University, Québec City, Québec, Canada; †Stephenson Cardiovascular Magnetic Resonance Centre at the Libin Cardiovascular Institute of Alberta, University of Calgary, Calgary, Alberta, Canada; ‡Siemens Canada Ltd., Calgary, Alberta, Canada; and the §Imaging Program, Lawson Health Research Institute, St. Joseph's Hospital, University of Western Ontario, London, Ontario, Canada. Dr. Friedrich is currently affiliated with the Montreal Heart Institute, Department of Cardiology, Université de Montréal, Montréal, Québec, Canada. During this study, Dr. Kumar was a Canadian Institutes of Health Research (CIHR) strategic training fellow in TORCH (Tomorrow's Research in Cardiovascular Health Professionals). Dr. Green is an employee of Siemens Canada Ltd. Dr. Friedrich is a shareholder and scientific advisor for Circle CVI, Calgary, Alberta, Canada. All other authors have reported that they have no relationships relevant to the contents of this paper to disclose.

Manuscript received December 15, 2010; revised manuscript received July 18, 2011, accepted August 23, 2011.

The success of reperfusion therapy in ST-elevation myocardial infarction is often diminished by a persistent post-procedural reduction of tissue perfusion at a microvascular level (1,2). This phenomenon related to reperfusion injury is characterized by 2 major components: microvascular obstruction (MO) and reperfusion hemorrhage.

MO was first described in the myocardium by Kloner et al. (3) and has since been investigated in patients with several imaging modalities (e.g., Thrombolysis In Myocardial Infarction flow or frame count [4–6], myocardial blush grade [5], coronary Doppler imaging [7], contrast echocardiography [8,9], and contrast-enhanced cardiac magnetic resonance [CMR] [2,10,11]). It was consistently associated with an adverse outcome for patients, including impaired functional recovery and increased mortality (1,2,12–17).

In contrast to MO, there is no validated imaging method for reperfusion hemorrhage in vivo, and therefore the specific role of hemorrhage as a contributor to reperfusion injury in humans remains ill-defined.

In images acquired by T2*-weighted magnetic resonance sequences, the regional signal intensity (SI) drops in hemorrhagic tissue because of altered molecular magnetic properties of hemoglobin degradation products (18,19). T2*-weighted imaging has become a clinical standard in the evaluation of hemorrhagic stroke (20–22), and initial reports for imaging myocardial hemorrhage in patients demonstrated feasibility for cardiac imaging (23). However, validation of T2*-weighted CMR (T2*-CMR) for myocardial hemorrhage using an ex vivo gold standard has yet to be performed, and therefore the diagnostic accuracy remains unclear.

The primary aim of this study was to validate the accuracy of T2*-CMR for the detection of ischemia/reperfusion injury–related myocardial hemorrhage in canines in vivo, when compared to ex vivo pathology. As a secondary goal, we also investigated the relationship of hemorrhage to MO, infarct size, ventricular volumes, and function.

METHODS

Animal model of reperfused myocardial infarction. The animal study was performed in 14 female mongrel dogs (weight 19 to 23 kg). The study was approved by the University of Western Ontario Council on Animal Care (Animal Use Subcommittee).

After 12 h of fasting, the dogs were anesthetized, intubated, and ventilated. Fentanyl citrate at 20 to 50 $\mu g \times$ h/kg was maintained for pain control; electrocardiogram (ECG) and blood pressure were monitored. Ventricular arrhythmia was controlled by boluses of lidocaine 1 mg/kg. After open thoracotomy, the left anterior descending coronary artery was ligated distal to the first diagonal branch for 3 to 4 h. The pericardium was reapproximated, and the chest closed. The dogs were extubated and allowed to recover; pain was controlled with a fentanyl patch for 48 h. At day 3 post–reperfused myocardial infarction, an in vivo CMR study and an ex vivo pathology study were performed.

In vivo CMR. CMR was performed on a 1.5-T system (Magnetom Avanto, Siemens Healthcare, Erlangen, Germany) using a 6-channel, phased-array cardiac coil (body coil for T2* acquisitions), under anesthesia and intubation/ventilation. All images were acquired using ECG triggering and applying breath-hold maneuvers by halting the ventilator for the time of image acquisition. The animals' heart rates were between 90 and 115 min^{-1}, and breath-hold durations were <18 s for all CMR image acquisitions.

ABBREVIATIONS AND ACRONYMS

CMR = cardiac magnetic resonance

ECG = electrocardiogram

IR-GE = inversion-recovery gradient echo

MO = microvascular obstruction

SI = signal intensity

TTC = triphenyl-tetrazolium chloride

After standard localization sequences, the following CMR sequences were applied in short-axis views, with a slice thickness of 10 mm with 0 gap, covering the entire left ventricle. For ventricular volumes and function, a steady-state free-precession (SSFP) sequence was used. For imaging myocardial hemorrhage, using the body coil, and after regional shimming, we applied a T2*-weighted gradient echo sequence with echo-planar readout, flip angle of 90°, effective echo time of 35 ms, ECG-triggered to mid-diastole, acquisition window of 72 ms, and an echo-planar imaging factor of 29. The total image data acquisition required 5 heart beats using a trigger pulse of 1 R-R interval. Typical values were: field of view, 350 × 17 mm; matrix, 256 × 128; and the resulting in-plane resolution, 1.4 × 1.4 mm. Because a body coil was used for T2*-CMR images, we did not apply surface coil intensity profile correction or pre-scan normalization. For visualizing MO, we used an inversion-recovery gradient echo (IR-GE) sequence 1.5 to 4 min after injection of 0.1 mmol/kg body weight of gadolinium-DTPA (Magnevist, Bayer Health Care, Toronto, Ontario, Canada) (2). For assessing myocardial necrosis, the same IR-GE was applied for 10 to 15 min post–

contrast injection, with an inversion time optimized to null signal from remote myocardium (late gadolinium enhancement) (24,25).

CMR image analysis. CMR images of a given sequence were analyzed by an observer blinded to the results of the other sequences and blinded to ex vivo images using certified software (cmr[42], Circle CVI, Calgary, Alberta, Canada). A standard slice-summation method was used to analyze SSFP cine images for left ventricular (LV) volumes and function. For tissue characterization, a semiautomated threshold-based detection method was used: Endocardial and epicardial borders were traced manually, and a region of interest was drawn in the myocardium opposite the infarcted area in the inferior wall. In the T2* and early post-contrast IR-GE images, the software automatically displayed areas of hemorrhage and MO, as defined by a SI of >2 SDs below the mean SI of remote tissue. A threshold of >5 SDs above the mean of remote myocardium was applied for late enhancement images (26,27). The volumetric extent of pathological tissue was measured. In addition, segmental involvement of hemorrhage was assessed using 6 segments per slice. The amount of hemorrhage was also measured as a percentage per slice for comparison with ex vivo data.

Image contrast was calculated using the following formula: Contrast = $[(SI_{\text{remote myocardium}} - SI_{\text{hemorrhagic myocardium}})/SI_{\text{remote myocardium}} \times 100\%]$ (28).

Susceptibility artifacts on T2*-CMR were defined a priori as areas of reduced or increased signal, which crossed anatomical borders, included the epicardial surface at the interface of myocardium, pericardium, and surrounding tissues, and could not be explained by adjacent anatomy (29,30) (Fig. 1). All artifacts were registered but excluded from the analysis of hemorrhage.

Ex vivo studies. After the CMR study, the dogs were maintained in general anesthesia, the chest was reopened, and 20 ml of a 4% thioflavin S solution was injected into the left atrium for subsequent imaging of MO. The dogs were euthanized, the hearts excised, and the myocardium was sectioned into short-axis slices of 10-mm thickness. Thioflavin S imaging for MO was performed using a digital camera with a band-pass filter for fluorescent signal. Thioflavin S stains endothelium in perfused blood vessels, and myocardium subject to MO remains unstained (31,32). Subsequently, triphenyl-tetrazolium chloride (TTC) staining was performed for hemorrhage and necrosis. TTC stains healthy myocardium brick red. Necrotic myocardium is not stained and appears pale white; hemorrhage within the necrosis zone appears dark red (32–34). The slices were digitally photographed.

Images of thioflavin S and TTC-stained slices were quantified using digital image analysis software (35). After careful optimization of image display for contrast and brightness, and enlarging the size for optimal visualization of tissue pathology, regions of interest were drawn manually in software using a contour tool, delineating tissue pathology (MO on thioflavin S images, necrosis and hemorrhage on TTC images). Areas of pathology were measured for each slice as percentage of all pixels representative of myocardium.

Before analysis, one observer matched in vivo and ex vivo image slices to be compared, using slice position information and anatomical landmarks. This observer was subsequently blinded by not having access to the data for 2 months.

Comparative assessment of tissue pathology. Using the methods described here, in vivo measurements of hemorrhage on T2*-CMR were compared with ex vivo hemorrhage on TTC images for segmental involvement and for percent myocardium involved per slice. The different tissue pathologies of MO, hemorrhage, and necrosis were compared with regard to their relative extent and involvement of total myocardium, and LV functional and volumetric data were compared for groups expressing different combinations of tissue pathology.

Clinical translation. To gain a preliminary impression of potential clinical applicability, we applied a similar imaging protocol using T2*-CMR in a small cohort of patients (n = 5) with late reperfused MI. Because of the small sample, results were not systematically analyzed.

Statistics. Data are expressed as mean ± SE. Segmental involvement of hemorrhage was compared in vivo and ex vivo using kappa agreement statistics. For assessing the relationship between continuous variables, Pearson correlation coefficient and linear regression analysis were performed. Differences between in vivo and ex vivo measurements were analyzed with a Bland-Altman plot. A Kolmogorov-Smirnov test was used to test the normal distribution of data. To compare continuous variables, a Student *t* test or Mann-Whitney *U* test was used, depending on the distribution of data. Multiplicity correction was not performed, but the analysis of hemorrhage size took into consideration that image slices with hemorrhage were not independent but originated from a limited number of animals.

Figure 1. Corresponding Images of Short Axis Slice From One (Top Panel) Dog With Nonhemorrhagic Infarction and 4 Dogs With Hemorrhagic Infarction

On the triphenyl-tetrazolium chloride (TTC) stain, a large anterior and lateral myocardial infarct is visible in all cases. The infarcted tissue is pale without evidence of hemorrhage in the **upper panels**, while the hemorrhage is visible in the subendocardium of the TTC-stained slice in the **lower panels (images on the very left**; **black arrows)**. The thioflavin S images **(second from left)** show normal fluorescent signal without evidence for a perfusion abnormality in most of the myocardium, but there is an absence of thioflavin S signal in the subendocardium/mid-myocardium of the anterior/lateral walls, consistent with microvascular obstruction in those areas. The corresponding T2*-cardiac magnetic resonance (CMR) images for hemorrhage show a homogenous signal without regional signal decrease in the nonhemorrhagic infarction **(upper panels)**, but a signal decrease reflecting the area of hemorrhage in hemorrhagic infarction **(white arrows**, **panels 2–5)**. Occasional susceptibility artifacts lead to a signal decrease on T2* that crosses anatomical borders **(asterisks)**. LGE = late gadolinium-enhanced image.

RESULTS

From 14 dogs examined, 1 lacked detectable necrosis on both late enhancement and TTC imaging and was excluded from the analysis. Thirteen dogs were available for analysis, and all demonstrated evidence of myocardial necrosis. Those were divided into 3 groups: 5 had myocardial infarction

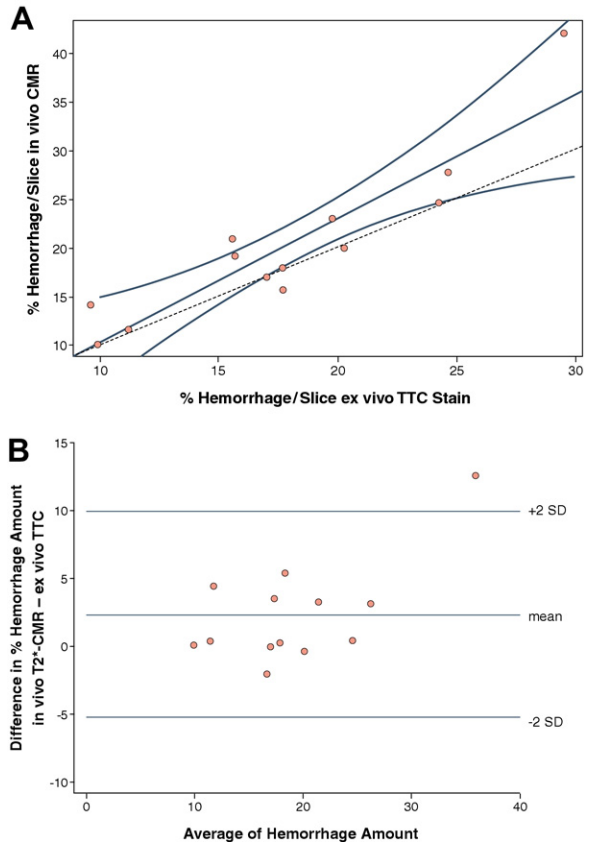

Figure 2. Plot of the Linear Regression Analysis and Bland-Altman Plot for In Vivo/Ex Vivo Comparison of the Extent of Reperfusion Hemorrhage

The extent of hemorrhage was measured as a percentage of total myocardium per slice. **A** shows linear regression analysis. The **solid lines** are the regression line based on the study data and their confidence bands; the **dotted line** represents the reference line of equality (slope 1.0). The in vivo T2*-CMR measurement of hemorrhage correlated well with hemorrhage on ex vivo TTC staining ($r^2 = 0.83$; $p < 0.01$). The slope of the regression line is 1.27 (95% confidence interval: 0.98 to 1.56).
B shows Bland-Altman plot. In repeated measurements, there was no significant difference in hemorrhage size (mean difference 2.39%, $p = 0.194$ [95% confidence interval: −2.17 to 6.96]). Abbreviations as in Figure 1.

without evidence of microvascular injury in vivo and ex vivo (MO- group). Eight dogs had MO on both early post-contrast IR-GE CMR and thioflavin S imaging: 4 dogs with MO but without reperfusion hemorrhage (MO+H- group) and 4 with MO and reperfusion hemorrhage (MO+H+ group). No dog had hemorrhage in the absence of MO. Examples of 1 nonhemorrhagic and all hemorrhagic infarctions are shown in Figure 1.

Comparison of hemorrhage in vivo versus ex vivo. Sixty-four slices could be successfully matched for in vivo/ex vivo comparison: 46 slices showed necrosis on TTC staining, 28 showed MO on thioflavin S staining, and 13 slices (from 4 dogs) showed hemorrhage on TTC staining. All slices with hemorrhage on TTC staining also had MO on thioflavin S staining.

The in vivo T2*-weighted CMR sequence yielded a contrast of 58 ± 19 for hemorrhagic versus remote myocardium. Overall, 384 segments were available for analysis, but 36 segments (9%) were excluded due to image artifacts, leaving 348 segments for analysis. From 40 hemorrhagic segments on TTC staining, 37 were positive on T2*-CMR. The kappa value for in vivo/ex vivo segmental agreement was 0.96 ($p < 0.01$).

In 13 slices affected by hemorrhage, the mean hemorrhage volume was 20.3 ± 2.3% per slice on the in vivo T2*-CMR images, and 17.9 ± 1.6% per slice on ex vivo TTC images. The values correlated well ($r = 0.91$; $p < 0.01$). Taking into account multiple measurements in 4 dogs, there was no significant difference between the amount of hemorrhage: the mean difference between T2*-CMR and TTC was 2.39 ± 1.43% ($p = 0.194$; 95% confidence interval: −2.17 to 6.96) (Fig. 2). The linear regression analysis yielded $r^2 = 0.83$ ($p < 0.01$) (Fig. 2A). The slope of the regression curve was 1.27 (95% confidence interval: 0.98 to 1.56).

Relation of hemorrhage to MO and necrosis CMR image analysis. Infarct size on late enhancement CMR in all dogs was 7.9 ± 2.6 g. MO in all dogs comprised 5.0 ± 1.5 g (8.4 ± 1.3 g in dogs with hemorrhage), and hemorrhage extent measured 6.1 ± 0.3 g. The amount of hemorrhage was smaller than the amount of MO in all dogs (mean difference 2.3 ± 1.0 g). The extent of necrosis correlated well with the extent of MO ($r = 0.77$; $p < 0.05$), the extent of MO correlated well with the extent of hemorrhage ($r = 0.87$; $p < 0.05$), and there was a moderate correlation between the extent of necrosis and the extent of hemorrhage ($r = 0.56$; $p < 0.05$).

Infarct size was larger in the subgroup with hemorrhage MO+H+ when compared with both other subgroups MO- and MO+H- (MO- 1.9 ± 1.4 g; MO+H- 4.1 ± 1.8 g; MO+H+ 19.3 ± 4.0 g; $p < 0.05$ for comparison of means of MO+H+ vs. both other groups [Fig. 3]). The amount of MO was larger in the group with hemorrhage than in the nonhemorrhage group (MO+H- 1.6 ± 0.7 g vs. MO+H+ 8.4 ± 1.3 g; $p < 0.05$ [Fig. 3]). In fact, hemorrhage was confined in this study to the 4 dogs that had both the largest infarcts and also the largest amount of MO (Fig. 4).

LV functional data were obtained from all dogs except for 1 due to an incomplete cine CMR dataset (hemorrhage group). Mean LV ejection fraction was lower in dogs with hemorrhage compared with dogs with MO but without hemorrhage (MO+H- 52 ± 7% vs. MO+H+ 28 ± 4%; $p < 0.05$). Cardiac output was lower in dogs with hemorrhage compared with dogs with MO but without hemorrhage (MO+H- 2.7 ± 0.2 l min^{-1} vs. MO+H+ 1.9 ± 0.1 l min^{-1}; $p < 0.05$). Mean LV end-diastolic volume was 71 ± 13 ml and did not differ among groups. Mean LV mass in all dogs was 75 ± 15 g and was higher in the MO+H+ group compared with the combination of the MO- and MO+H- groups (90 ± 13 g vs. 70 ± 12 g; $p < 0.05$).

Ex vivo analysis. The results of the ex vivo analysis are summarized in Table 1. Infarct-related necrosis covered a mean of 16.8 ± 2.4% of the myocardium per slice considering all slices with necrosis. Comparing the ex vivo TTC-stained slices according to the subgroups described earlier, the MO- group had less necrosis per slice than the MO+H- group, which again had less necrosis per slice than the MO+H+ group (mean amount of tissue necrosis per slice: MO- 5.1 ± 1.6%; MO+H- 11.3 ± 1.5%; MO+H+ 38.8 ± 2.8%; $p < 0.05$ for all comparisons). For MO, a larger percentage of MO per slice was observed in slices with hemorrhage (n = 13) compared with slices without hemorrhage (n = 15) (MO+H- 7.8 ± 1.4% per slice vs. MO+H+ 27.4 ± 2.3% per slice; $p < 0.0001$). Hemorrhage occupied a mean of 17.9 ± 1.6% of myocardium in affected slices (n = 13).

The area of necrosis was consistently larger than the area of MO (mean difference 7.2 ± 1.3% of myocardium per slice). The region with MO was consistently larger than that of hemorrhage (mean difference 8.8 ± 2.0% of myocardium per slice).

Clinical translation. We observed hemorrhage in 3 of 5 patients with acute myocardial infarction who received reperfusion therapy >8 h after onset of chest pain. Example images of a patient are presented in Figure 5.

DISCUSSION

We demonstrated that in vivo T2*-CMR accurately quantifies myocardial hemorrhage post-reperfusion in acute myocardial infarction compared with an ex vivo gold standard. Hemorrhage is located in the core of the infarction, mainly subendocardial, embedded within the zone of MO. Hemorrhage did not occur without MO, was associated with larger myocardial infarction, more extensive MO, and greater reduction of LV systolic function.

Our data provide the first systematic in vivo/ex vivo validation of T2*-CMR for the assessment of reperfusion hemorrhage. There are previous reports (without in vivo/ex vivo validation) that suggested the use of T2-weighted spin-echo sequences (36–38) for detecting hemorrhage.

Although magnetic susceptibility effects stemming from hemoglobin degradation products may lead to reduced signal in T2 images, the T2* effects

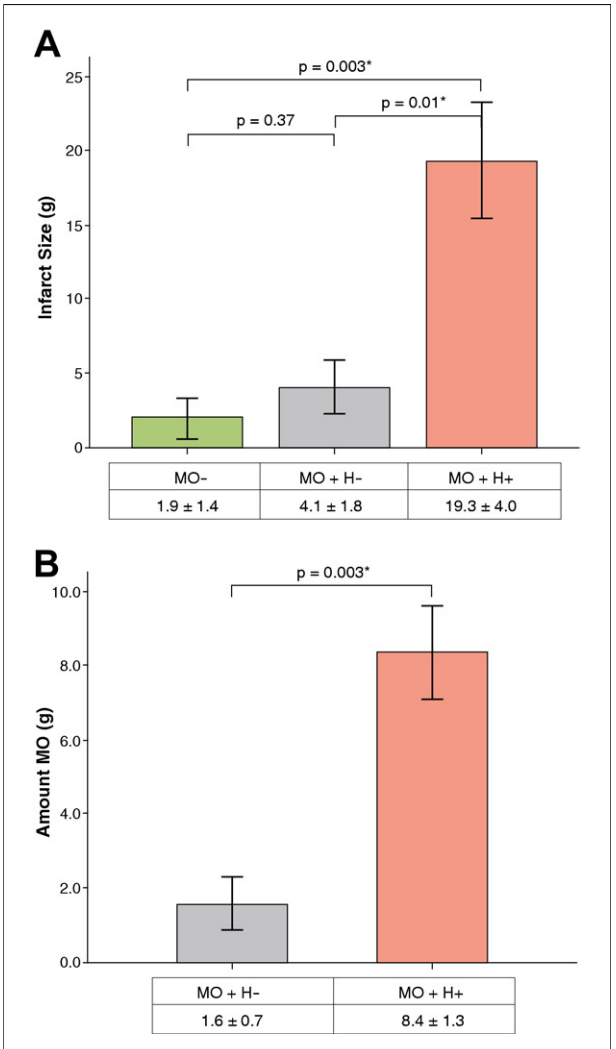

Figure 3. Overview of In Vivo CMR Parameters Divided According to Subgroups

Dogs with hemorrhage (MO+H+) had **(A)** larger infarctions and **(B)** more MO. Significant p values are marked with an **asterisk**. Values are mean ± 1 SE. H = reperfusion hemorrhage; MO = microvascular obstruction; other abbreviation as in Figure 1.

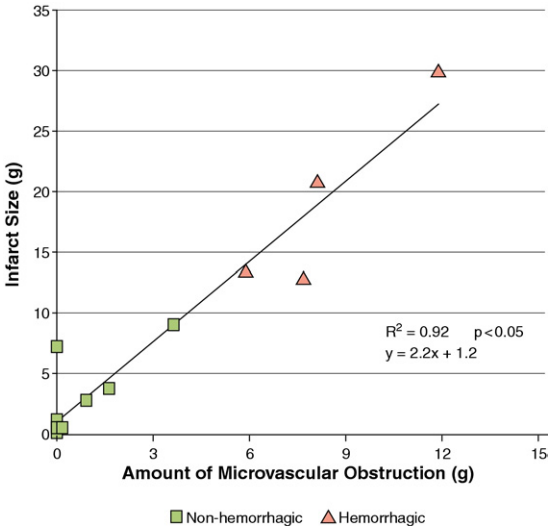

Figure 4. Relationship of Hemorrhagic and Nonhemorrhagic Myocardial Infarcts to the Amount of MO and Infarct Size as Measured by In Vivo CMR

The hemorrhagic and nonhemorrhagic groups are distinct, with hemorrhage occurring exclusively in the 4 dogs with the largest infarcts as well as the greatest amount of MO. Abbreviations as in Figures 1 and 3.

are substantially greater. The principal mechanism augmenting T2* sensitivity to such off-resonance effects is the absence of any radiofrequency refocusing pulses that lead to an accelerated loss of phase coherence among spins (39). T2*-CMR was recently applied to assess hemorrhage in patients (23), but so far there is no in vivo/ex vivo validation available.

Pathophysiological aspects. Our results provide the first in vivo confirmation of previous ex vivo work; earlier ex vivo studies have suggested that hemorrhage may occur as a complication of MO (40,41). In line with this observation, we observed in vivo hemorrhage within the MO zone, and the extent of hemorrhage was smaller than the extent of MO. Furthermore, few dogs had MO without hemorrhage.

We observed a linear relationship between the extent of necrosis, MO, and hemorrhage, suggesting that these components of tissue injury are not independent of each other, and that there could perhaps be a causal relationship. Hemorrhage occurred only in infarcts with the most extensive MO and the largest infarct size (both around 4 times larger than infarcts with MO but without hemorrhage), suggesting that the amount and severity of tissue injury may be a predisposing factor for the development of hemorrhage. Although CMR already provides imaging tools for the first 3 major components of tissue injury (edema [T2-weighted CMR], cardiomyocyte necrosis [late enhancement CMR], and MO [early IR-GE CMR]), our data indicate that T2*-weighted imaging provides an additional noninvasive imaging tool for the fourth major component of acute tissue injury, myocardial hemorrhage.

Imaging aspects. Theoretically, a small overestimation of in vivo hemorrhage measurements with T2*-CMR had been expected, explained by magnetic field effects related to hemorrhage exceeding the spatial extent of hemorrhage. Also, CMR delivers a summation signal from the entire slice thickness while ex vivo pathology delivers surface images. Nevertheless, hemorrhage size did not differ between in vivo and ex vivo measurements when taking into account multiple measurements in 4 dogs. TTC staining was used here as a reference standard for macroscopic hemorrhage, as established previously (32,40,41); we did not perform histology for microscopic hemorrhage. Although studies with a larger sample size could help to determine potential differences between T2*-CMR for in vivo hemorrhage and hemorrhage on ex vivo pathology, we expect that those may be small and perhaps not clinically important because hemorrhage size was similar by T2* in vivo and ex vivo TTC in this study.

We found a relatively high incidence of artifacts (9% of all segments). In our study, these artifacts were easy to identify (usually epicardial, "penetrating" anatomical structures) (29,30) and did not interfere with hemorrhage signal analysis.

Table 1. Ex Vivo Imaging Data for Necrosis, Microvascular Obstruction, and Hemorrhage

	All	MO-	MO+ H-	MO+ H+	p Value
TTC % necrosis	16.8 ± 2.4	5.1 ± 1.6	11.3 ± 1.5	38.8 ± 2.8	<0.05 for all subgroups
Thioflavin S % MO		—	7.8 ± 1.4	27.4 ± 2.3	0.0001
TTC % hemorrhage		—	—	17.9 ± 1.6	NA

Values are mean ± SD. Hemorrhage was smaller than the amount of MO. In slices with hemorrhage, there was a greater extent of MO and necrosis compared with nonhemorrhagic slices. Extent measured as mean percentage per slice ± SEM.
MO = microvascular obstruction; NA = not applicable; NS = not significant; TTC = triphenyl-tetrazolium chloride.

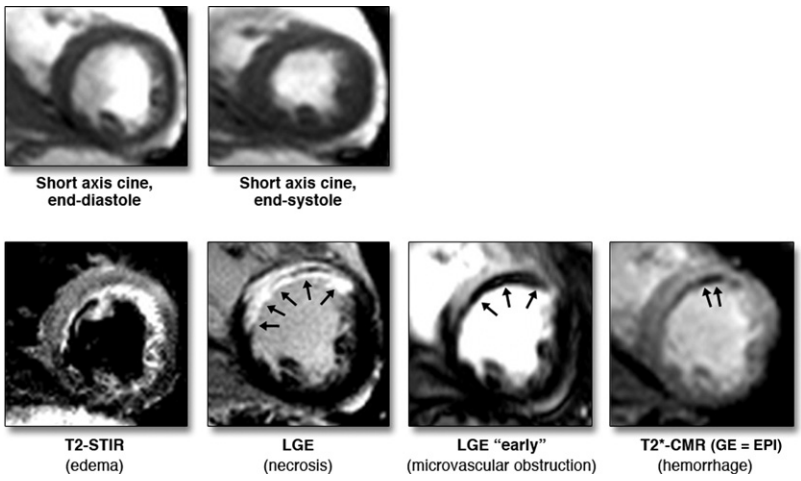

Figure 5. Midventricular Short-Axis Views of a Patient With Late Reperfused Acute Myocardial Infarction

(Upper panel) Short-axis cine snapshots of an end-diastolic and end-systolic frame demonstrating anteroseptal akinesis. **(Lower panel: extreme left)** Pre-contrast T2-STIR imaging showing high signal in the anteroseptal wall consistent with myocardial edema. **(Middle left)** Post-contrast (>10 min) LGE showing a nearly transmural anteroseptal myocardial infarction. **(Middle right)** LGE sequence applied early after contrast injection (2 to 3 min) reveals a large area of microvascular obstruction **(arrows)**. **(Extreme right)** Pre-contrast T2*-CMR image shows an area of subendocardial low signal within the microvascular obstruction zone consistent with myocardial hemorrhage (arrows). GE-EPI = gradient echo with echo-planar image readout; T2-STIR = T2-weighted short tau inversion recovery; other abbreviations as in Figure 1.

Theoretically, a problem could occur in a very large myocardial infarction with transmural hemorrhage fusing with an epicardial susceptibility artifact that accidentally occurs in the same segment. We did not encounter this scenario in our study.

Finally, it has to be expected that advances in sequence development (e.g., T2*-prepared SSFP sequences, T2* mapping) will be able to reduce image artifacts while maintaining sufficient T2* sensitivity for imaging hemorrhage in the future.

Clinical implications. This approach provides means to shed light on myocardial hemorrhage as a complication of ischemia/reperfusion injury in acute myocardial infarction. The implications of hemorrhage, including its incidence, possible adverse effects on LV remodeling, and patient prognosis, can now be studied in patients without the use of a contrast agent. The protective or facilitating effects of drugs such as thrombolytic agents, anticoagulants, and platelet aggregation inhibitors on myocardial hemorrhage may now be investigated using T2*-weighted CMR in patients.

Although LV systolic function was most compromised in the hemorrhagic infarction group, this study was not powered to determine whether this effect is independent of other determinants of ventricular function, such as infarct size and MO.

CONCLUSIONS

We conclude that T2*-CMR accurately detected and quantified myocardial hemorrhage in vivo and provides a tool to noninvasively investigate myocardial hemorrhage as a novel diagnostic target in myocardial reperfusion injury. Our data suggest that hemorrhage occurs as a consequence of reperfusion in more advanced myocardial infarctions and may therefore be a marker of more severe tissue injury.

Acknowledgments

The authors thank Dr. Sarah Rose for statistical advice and Ms. Jacqueline Flewitt and Dr. James Hare for their critical revision of the manuscript.

Reprint requests and correspondence: Dr. Matthias G. Friedrich, Stephenson Cardiovascular Magnetic Resonance Centre at the Libin Cardiovascular Institute of Alberta, University of Calgary, FMC Suite 0700-SSB-1403, 29th Street NW, Calgary, Alberta T2N 2T9, Canada. *E-mail: mgwfriedrich@gmail.com.*

REFERENCES

1. Ito H. No-reflow phenomenon and prognosis in patients with acute myocardial infarction. Nat Clin Pract Cardiovasc Med 2006;3:499–506.
2. Wu KC, Zerhouni EA, Judd RM, et al. Prognostic significance of microvascular obstruction by magnetic resonance imaging in patients with acute myocardial infarction. Circulation 1998;97:765–72.
3. Kloner RA, Ganote CE, Jennings RB. The "no-reflow" phenomenon after temporary coronary occlusion in the dog. J Clin Invest 1974;54:1496–508.
4. Ito H, Okamura A, Iwakura K, et al. Myocardial perfusion patterns related to thrombolysis in myocardial infarction perfusion grades after coronary angioplasty in patients with acute anterior wall myocardial infarction. Circulation 1996;93:1993–9.
5. Gibson CM, Cannon CP, Murphy SA, et al. Relationship of TIMI myocardial perfusion grade to mortality after administration of thrombolytic drugs. Circulation 2000;101:125–30.
6. Gibson CM, Murphy SA, Rizzo MJ, et al. Relationship between TIMI frame count and clinical outcomes after thrombolytic administration. Thrombolysis In Myocardial Infarction (TIMI) Study Group. Circulation 1999;99:1945–50.
7. Iwakura K, Ito H, Takiuchi S, et al. Alternation in the coronary blood flow velocity pattern in patients with no reflow and reperfused acute myocardial infarction. Circulation 1996;94:1269–75.
8. Ito H, Tomooka T, Sakai N, et al. Lack of myocardial perfusion immediately after successful thrombolysis. A predictor of poor recovery of left ventricular function in anterior myocardial infarction. Circulation 1992;85:1699–705.
9. Kaul S. Evaluating the 'no reflow' phenomenon with myocardial contrast echocardiography. Basic Res Cardiol 2006;101:391–9.
10. Wu KC, Kim RJ, Bluemke DA, et al. Quantification and time course of microvascular obstruction by contrast-enhanced echocardiography and magnetic resonance imaging following acute myocardial infarction and reperfusion. J Am Coll Cardiol 1998;32:1756–64.
11. Rochitte CE, Lima JA, Bluemke DA, et al. Magnitude and time course of microvascular obstruction and tissue injury after acute myocardial infarction. Circulation 1998;98:1006–14.
12. The effects of tissue plasminogen activator, streptokinase, or both on coronary-artery patency, ventricular function, and survival after acute myocardial infarction. The GUSTO Angiographic Investigators. N Engl J Med 1993;329:1615–22.
13. Porter TR, Li S, Oster R, Deligonul U. The clinical implications of no reflow demonstrated with intravenous perfluorocarbon containing microbubbles following restoration of Thrombolysis In Myocardial Infarction (TIMI) 3 flow in patients with acute myocardial infarction. Am J Cardiol 1998;82:1173–7.
14. Hombach V, Grebe O, Merkle N, et al. Sequelae of acute myocardial infarction regarding cardiac structure and function and their prognostic significance as assessed by magnetic resonance imaging. Eur Heart J 2005;26:549–7.
15. Morishima I, Sone T, Okumura K, et al. Angiographic no-reflow phenomenon as a predictor of adverse long-term outcome in patients treated with percutaneous transluminal coronary angioplasty for first acute myocardial infarction. J Am Coll Cardiol 2000;36:1202–9.
16. Swinburn JM, Lahiri A, Senior R. Intravenous myocardial contrast echocardiography predicts recovery of dysynergic myocardium early after acute myocardial infarction. J Am Coll Cardiol 2001;38:19–25.
17. Smith DF, Higginson LA, Walley VM. Reperfusion hemorrhage following PTCA and thrombolysis for left main coronary artery occlusion. Can J Cardiol 1988;4:33–6.
18. Pauling L, Coryell CD. The magnetic properties and structure of the hemochromogens and related substances. Proc Natl Acad Sci U S A 1936;22:159–63.
19. Bradley WG Jr. MR appearance of hemorrhage in the brain. Radiology 1993;189:15–26.
20. Linfante I, Llinas RH, Caplan LR, Warach S. MRI features of intracerebral hemorrhage within 2 hours from symptom onset. Stroke 1999;30:2263–7.
21. Hermier M, Nighoghossian N. Contribution of susceptibility-weighted imaging to acute stroke assessment. Stroke 2004;35:1989–94.
22. Chalela JA, Kidwell CS, Nentwich LM, et al. Magnetic resonance imaging and computed tomography in emergency assessment of patients with suspected acute stroke: a prospective comparison. Lancet 2007;369:293–8.
23. O'Regan DP, Ahmed R, Karunanithy N, et al. Reperfusion hemorrhage following acute myocardial infarction: assessment with T2* mapping and effect on measuring the area at risk. Radiology 2009;250:916–22.
24. Simonetti OP, Kim RJ, Fieno DS, et al. An improved MR imaging technique for the visualization of myocardial infarction. Radiology 2001;218:215–23.
25. Kim RJ, Fieno DS, Parrish TB, et al. Relationship of MRI delayed contrast enhancement to irreversible injury, infarct age, and contractile function. Circulation 1999;100:1992–2002.
26. Bondarenko O, Beek AM, Hofman MB, et al. Standardizing the definition of hyperenhancement in the quantitative assessment of infarct size and myocardial viability using delayed contrast-enhanced CMR. J Cardiovasc Magn Reson 2005;7:481–5.
27. Amado LC, Gerber BL, Gupta SN, et al. Accurate and objective infarct sizing by contrast-enhanced magnetic resonance imaging in a canine myocardial infarction model. J Am Coll Cardiol 2004;44:2383–9.
28. Peli E. Contrast in complex images. J Opt Soc Am A. 1990;7:2032–40.
29. Atalay MK, Poncelet BP, Kantor HL, Brady TJ, Weisskoff RM. Cardiac susceptibility artifacts arising from the heart-lung interface. Magn Reson Med 2001;45:341–5.
30. Ludeke KM, Roschmann P, Tischler R. Susceptibility artefacts in NMR imaging. Magn Reson Imaging 1985;3:329–43.
31. Schlegel JU. Demonstration of blood vessels and lymphatics with a fluorescent dye in ultraviolet light. Anat Rec 1949;105:433–43.
32. Kloner RA, Alker KJ. The effect of streptokinase on intramyocardial hemorrhage, infarct size, and the no-reflow phenomenon during coronary reperfusion. Circulation 1984;70:513–21.
33. Fishbein MC, Meerbaum S, Rit J, et al. Early phase acute myocardial infarct size quantification: validation of the triphenyl tetrazolium chloride tissue enzyme staining technique. Am Heart J 1981;101:593–600.
34. Pitts KR, Stiko A, Buetow B, et al. Washout of heme-containing proteins dramatically improves tetrazolium-based infarct staining. J Pharmacol Toxicol Methods 2007;55:201–8.
35. Rosset A, Spadola L, Ratib O. OsiriX: an open-source software for navigating in multidimensional DICOM images. J Digit Imaging 2004;17:205–16.
36. Lotan CS, Bouchard A, Cranney GB, Bishop SP, Pohost GM. Assessment of postreperfusion myocardial hemorrhage using proton NMR imaging at 1.5 T. Circulation 1992;86:1018–25.

37. Asanuma T, Tanabe K, Ochiai K, et al. Relationship between progressive microvascular damage and intramyocardial hemorrhage in patients with reperfused anterior myocardial infarction: myocardial contrast echocardiographic study. Circulation 1997;96: 448–53.
38. Ganame J, Messalli G, Dymarkowski S, et al. Impact of myocardial haemorrhage on left ventricular function and remodelling in patients with reperfused acute myocardial infarction. Eur Heart J 2009;30:1440–9.
39. Gillis P, Koenig SH. Transverse relaxation of solvent protons induced by magnetized spheres: application to ferritin, erythrocytes, and magnetite. Magn Reson Med 1987;5:323–5.
40. Fishbein MC, Y-Rit J, Lando U, Kanmatsuse K, Mercier JC, Ganz W. The relationship of vascular injury and myocardial hemorrhage to necrosis after reperfusion. Circulation 1980;62: 1274–9.
41. Reffelmann T, Kloner RA. Microvascular reperfusion injury: rapid expansion of anatomic no reflow during reperfusion in the rabbit. Am J Physiol Heart Circ Physiol 2002; 283:H1099–107.

Key Words: cardiac magnetic resonance ■ ischemia/reperfusion injury ■ microvascular obstruction ■ myocardial hemorrhage ■ myocardial infarction ■ myocardial reperfusion.